Revealing the effect of medium-range structure on silicate glass hardness

Ying Shi [1,*] Binghui Deng [1] Jörg Neuefeind,[2] Qi Zhou,[3] Morten M. Smedskjaer [4] Stephen R. Elliott,[5] and Mathieu Bauchy[3]

[1]*Science and Technology Division, Corning Incorporated, Corning, New York 14831, USA*
[2]*Neutron Scattering Division, Spallation Neutron Source (SNS), Oak Ridge National Laboratory, Oak Ridge, Tennessee 37831, USA*
[3]*Physics of AmoRphous and Inorganic Solids Laboratory (PARISlab), Department of Civil and Environmental Engineering, University of California, Los Angeles, California 90095, USA*
[4]*Department of Chemistry and Bioscience, Aalborg University, Aalborg, Denmark*
[5]*Physical and Theoretical Chemistry Laboratory, University of Oxford, Oxford OX1 3QZ, United Kingdom*

(Received 25 August 2022; accepted 5 December 2022; published 4 January 2023)

Atomic structure determines physical properties, but for glassy materials, the nature of structure-property relationships remains ambiguous. Since glass properties are governed by both chemistry and structure, it is difficult to dissociate these two effects. Here, the sole effect of the structure on property is isolated by treating an industrial aluminosilicate glass with either thermal-annealing or pressure-quenching processes to produce glasses with varying densities and hardnesses (at constant composition). To explore the underlying structural origin of property changes, neutron total-scattering patterns of these glasses were measured. These results confirm the applicability of rigid-unit mode theory since the short-range tetrahedra were found to remain unaffected. In contrast, close correlations are derived between properties and medium-range structure (as encoded in various features of the first sharp diffraction peak). Overall, it reveals that the increase in the medium-range order is the structural origin of the extra extent of hardness increase beyond the densification effects.

DOI: 10.1103/PhysRevMaterials.7.013602

I. INTRODUCTION

One of the fundamental principles in materials science—that atomic structure determines physical properties—is derived mainly from studies on crystalline materials. Blessed by the symmetry and periodicity of crystalline materials, crystallographers have been very successful in determining their structures and deciphering the underlying relationship with properties. However, structure-property correlations are far less well understood for glassy materials. Building a ternary composition-structure-property correlation has been the holy grail for glass scientists. With such knowledge, glass compositions could be formulated to achieve tailored properties, which otherwise tend to be developed by relying on Edisonian trial-and-error methods. In practice, it is common to simplify the ternary correlation by collapsing it into a binary one, i.e., composition-property, by omitting the key middle parameter—structure—even though such composition-property relationships are partially ill defined because glasses are out-of-equilibrium phases, and their properties depend on their formation history. This is, in some cases, a fair treatment since correlations can usually be found between properties and composition [1] or the composition-derived structural parameters such as packing fraction [2], nonbridging oxygen content for oxides glasses [1], or network-former coordination speciation by providing, e.g., the perfect interpretation of the boron anomaly in borate glasses [3,4]. The breakdown of such correlations has provoked intriguing and longstanding challenges in glass science. One such example is the well-known mixed-alkali [5,6] or alkaline-earth [7] effect. Another example is the abnormal deviation from linearity in the hardness of certain silicate glasses [8,9]. Only by considering the structural parameters can such breakdowns of correlations, i.e., the mysteries of nonadditive or abnormal behavior [10], be resolved.

Glasses do not have any long-range order and tend to exhibit a short-range order that is like that of their crystalline counterpart. Therefore, the key structural information lies in the medium range, which is primarily encoded in the ring-size distribution of network glasses. This leads to another practical reason for the omission of structural parameters: We have not previously had a reliable method to determine and quantify the medium-range structure in glasses until analytical methods have been proposed such as the recently developed [10] and validated [11] RingFSDP method. The heuristic RingFSDP method, developed from experimental data, aims to extract the ring-size distribution in silicate glasses from the shape of the first sharp diffraction peak (FSDP) of the neutron-scattering structure factor [10].

To study structure-property correlations, we choose to study hardness (H). Hardness is defined as the ability to resist permanent deformation [12], which is irreversible and involves microscale structural changes featuring nonaffine atomic rearrangements [13]. Therefore, hardness should be affected by both microscale structure and macroscale packing fraction. For simplicity, to filter out the effect of composition from the ternary composition-structure-property relationship,

*shiy3@corning.com

we consider an aluminosilicate glassy material (of fixed composition) that is experimentally treated by both sub$-T_g$ thermal-annealing and pressure-quenching processes [14]. In the same original study, classical molecular dynamics (MD) simulations were also used to generate thermally annealed and pressure-quenched glass structures to explore the associated microscale structural change [14]. The simulated, extreme high-density glass structures were generated by the thermal-annealing process and exhibited density values that are comparable with the ones derived by the pressure-quenching process, even though such high-density glasses could never be experimentally made by thermal-annealing treatments. MD simulations showed no significant changes in interatomic distances, coordination numbers, or Q^n distributions as a function of density in all simulated glass structures [14]. However, by comparing the simulated thermal-annealing and pressure-quenching structures with similar densities, it was shown that pressure quenching has a larger impact than thermal annealing on the medium-range structure, as shown by the decrease in the medium-range distances (MRDs). In contrast, the thermal-annealing process has a larger impact than pressure quenching on the short-range order as a more rigid short-range structure was observed upon thermal annealing—as shown by the sharper standard deviations of bond-angle distributions of both intratetrahedral (O-*A*-O) and intertetrahedral (*A*-O-*A*) angles with *A* representing glass formers as Si or Al. This more rigid short-range structure was then claimed to be the structural origin of the higher hardness of the same density glasses simulated by thermal annealing than the pressure-quenching process.

Here, we explore the nature of the structure-hardness relationship by studying the same sets of glasses experimentally produced by both sub-T_g thermal-annealing and pressure-quenching processes [14]. The treatments resulted in the formation of six glasses with various extents of densification and hardness increase. Unlike what was observed in previous simulations [14], the experimental thermal-annealing process does not result in any notable density change, while the pressure quench increases density significantly. In contrast, hardness increases upon both annealing and pressure, and for pressure-quenched glasses, the increase in hardness is more pronounced. For glasses with the same composition, the increase in density leads to a higher packing fraction and, thereby, a higher stiffness (Young's modulus) and hardness. However, the very different variations in ρ and H upon thermal annealing and pressurization clearly demonstrate that the increase in hardness does not solely arise from an increase in density. This implies that, in addition to the macroscale densification, there must be other factors contributing to the increase in hardness. This leads to the main motivation of this paper, i.e., experimentally identifying the microscale structural origin of the increase in hardness.

II. EXPERIMENT

A. Studied glasses and their properties

Here, we study the industrial alkaline-earth aluminosilicate glass, named *Jade* [15], with a nominal composition of $(CaO)_6(MgO)_7(Al_2O_3)_{13}(SiO_2)_{74}$. The as-prepared (AP) glass was manufactured by the fusion-draw process, which ensures homogeneity of the glass sheet. It also yields a high initial fictive temperature $T_f = 1125$ K for the AP glass, which allows a greater fictive temperature difference (91 K) between the AP and the subsequent heat treatment at 1034 K. The AP glass sheets, with dimensions of $\sim 25 \times 25 \times 0.7\,\text{mm}^3$, were treated by either a thermal-annealing or pressure-quenching process to produce glasses with increased density and hardness. Three annealed glasses were heated at $T_a = 0.98T_g$ ($T_g = 1055$ K) for three different duration times t_a (15, 180, and 960 min), then rapidly quenched to room temperature (RT). Three pressure-quenched glasses were isostatically compressed using a nitrogen-gas pressure chamber at T_g for 30 min at three pressures P(0.2, 0.6, and 1.0 GPa), cooled down to RT first, and then decompressed to ambient pressure. Density (ρ) and Vickers hardness (H) of all seven glasses (including an unannealed and unpressurized AP sample), listed in the Supplemental Material Table S1 [16], were measured and reported in Ref. [14]. Details of the pressure-quenching process and property measurements are described in Ref. [17]. Vickers hardness (H) of the samples was determined using a micro-indenter (Duramin 5, Struers A/S). A total of 30 indents were conducted on each sample using an indentation time of 10 s and an indentation load of 0.25 N. The measurements were performed in air at RT.

To illustrate the thermal and pressure effects on the glass properties, we calculate, based on the data in Ref. [14], the relative property change for each treated glass by comparing it with the corresponding AP glass, e.g., $\Delta\rho/\rho(\%) = (\rho_{\text{treated}} - \rho_{\text{AP}})/\rho_{\text{AP}} \times 100$. The relative changes in density (ρ) and Vickers hardness (H) are plotted in Figs. 1(a) and 1(b) as a function of their corresponding annealing duration (lower x axis) or compression pressure (upper x axis). As shown in Fig. 1(a), annealing does not notably change the density (red symbols), while pressure-quenched glasses show a linear density increase with pressure (blue symbols). In contrast, the hardness increases upon both annealing and pressure [Fig. 1(b)], although for pressure-quenched glasses, the increase in hardness is more pronounced. The very different ρ and H changes with thermal annealing and pressurization clearly demonstrate that the increase in hardness does not solely arise from an increase in density since (1) annealing does not induce a noticeable density change, but it increases the hardness by up to 6.2%; and (2) for the pressure-quenched glass at 1.0 GPa, its density increases by only 3.8%, while its hardness increases by up to 18.5%.

B. Neutron total-scattering measurement and normalization

Time-of-flight neutron-scattering measurements were performed on the Nanoscale-Ordered Materials Diffractometer (NOMAD) at the SNS, Oak Ridge National Laboratory [18]. Relevant experimental details are reported in Ref. [10]. The normalized neutron-reduced structure-factor functions $F(Q)$ $\{F(Q) = Q \cdot [S(Q) - 1]\}$ of the annealed and pressure-quenched glasses are presented in Figs. 2(a-1) and 2(a-2), respectively. The reduced pair-distribution functions $G(r)$ are obtained by direct Fourier transformation of $F(Q)$, according to $G(r) = (\frac{2}{\pi}) \int_0^{Q_{\max}} F(Q) \sin(Qr) dQ$

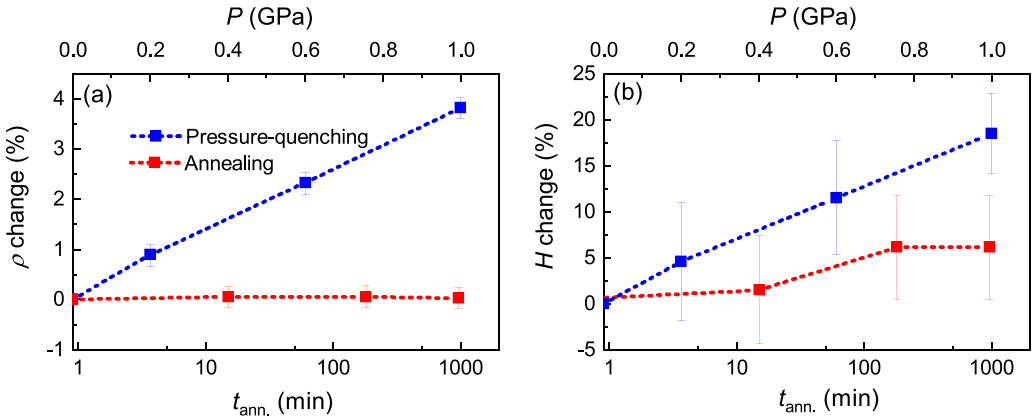

FIG. 1. Effects of thermal annealing (red) and pressure quenching (blue) on the change in (a) density (ρ) and (b) hardness (H). The relative change (%) is calculated by comparing the treated glass with the as-prepared one. Density does not notably change upon annealing but increases linearly with pressure for pressure-quenched glasses. Hardness increases upon both treatments. Both density and hardness data are from Ref. [14]. The errors in the density change are propagated from the density error of $\pm 0.004\,\mathrm{g/cm^3}$, as reported in Ref. [17]. The errors in the hardness change are propagated from the errors of hardness values estimated from fig. 2 of Ref. [14].

(where $Q_{\max} = 50\,\text{Å}^{-1}$). The corresponding $G(r)$ functions are plotted in Figs. 2(b-1) and 2(b-2).

As described below, structural information will be derived from an analysis of the FSDP of the structure factor, including the peak position, area, and shape. Therefore, it is critical to normalize the structure factor to the absolute correct scale. Here, this is accomplished by utilizing the low-r region of $G(r)$ criterion, as described in Ref. [19]. When r is smaller than the first atomic-pair peak in the pair distribution function (~ 1.65 Å, assigned as Si-O or Al-O peaks for Jade glass), the low-r region of $G(r)$ should theoretically be a straight line going through zero, with slope $-4\pi\rho_0$, where ρ_0 is the

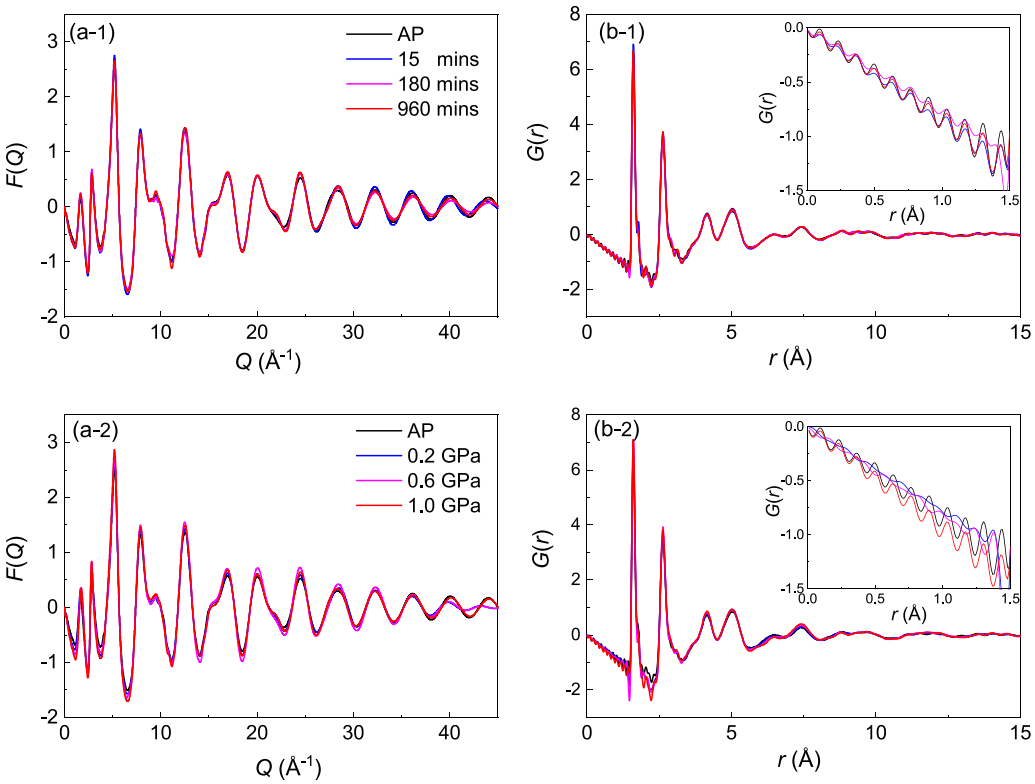

FIG. 2. (a-1) and (a-2) Normalized reduced structure-factor functions $F(Q)$ and (b-1) and (b-2) Fourier-transformed reduced pair distribution functions $G(r)$ for thermal-annealed (top panel) and pressure-quenched (bottom panel) glasses. The same color schemes as labeled in the $F(Q)$ plots are used in the $G(r)$ plots. Insert: Zoomed low-r region of $G(r)$ curves demonstrating the correct normalization of the $F(Q)$ scans, with similar slopes through the rippled $G(r)$ curves for the annealed glasses [insert of (b-1)] reflecting their comparable densities, whereas the higher negative slopes of the high pressure-quenched glasses [insert of (b-2)] reflect their higher density.

atomic number density, and linearly correlated with the mass density. In fact, as shown in the inserts of Figs. 2(b-1) and 2(b-2), the low-r part of the $G(r)$ curve contains small ripples, also named termination ripples, which are caused by Fourier-transforming the scattering data collected for a finite-Q range. The small ripples of $G(r)$ in the low-r region should oscillate around the theoretical straight low-r line. This is the low-r region of $G(r)$ criterion that can be used for absolute correct scale normalization. The correct normalizations are demonstrated in the inserts of Figs. 2(b-1) and 2(b-2). Similar slopes through the rippled $G(r)$ curves for the annealed glasses [insert of Fig. 2(b-1)] reflect their comparable densities, whereas the higher negative slopes of the pressure-quenched glasses treated at higher pressures [insert of Fig. (b-2)] reflect their higher density.

C. RingFSDP for medium-range structure

We have recently developed a method, RingFSDP, to quantify the ring-size distribution of silicate glasses from the FSDP of the neutron-scattering structure factor [10]. This method deconvolves the FSDP into three modified Gaussian peaks, with each peak ascribed to a certain family of rings: (i) large rings ($\geqslant$6-membered) centered at low Q; (ii) medium-sized rings (5-membered) centered at intermediate Q; and (iii) small rings ($\leqslant$4-membered) centered at large Q. The FSDP deconvolution, as well as ring-size distribution calculation, is performed using the Python program RingFSDP. A detailed step-by-step deconvolution procedure is described in the Supplemental Material [16] to demonstrate how RingFSDP works.

Since the shape of the FSDP is generally broad and asymmetric, the following two practices should be applied to ensure a reliable FSDP deconvolution. First, the $F_{\mathrm{FSDP}}(Q)$ in reciprocal space needs to be Fourier transformed into its real-space representation $I_{\mathrm{FSDP}}(r)$ since the latter expands the signal and allows for more reliable model fitting. Second, the deconvolution of FSDP is performed through the fitting of $I_{\mathrm{FSDP}}(r)$ by three compressed exponentially decaying sine waves in real space, which correspond to the three modified Gaussian peaks in reciprocal space. This fitting model was developed empirically from the fitting of the $I_{\mathrm{FSDP}}(r)$ profiles of 81 aluminosilicate glasses [10]. It was found that, in most fittings, the periodicities of the three sine waves generally converge to constant values, i.e., 3.15 ± 0.01, 3.70 ± 0.03, and 4.30 ± 0.04 Å, respectively, where the mean and standard deviation values are calculated from 81 glass fittings. Comparing with the ring-structure information of crystalline SiO_2 polymorphs, we postulate that the three characteristic periodicities ($r = 3.15$, 3.70, and 4.30 Å) correspond to the typical effective diameters of small ($\leqslant$4), intermediate (5), and large rings ($\geqslant$6), respectively [10].

Mathematically, the three periodicities of the sine waves in real space of $I_{\mathrm{FSDP}}(r)$ correspond to the three Gaussian peak positions of the $F_{\mathrm{FSDP}}(Q)$ deconvolution in reciprocal space, with Q values at 2.00, 1.70, and 1.46 Å^{-1}, respectively. More importantly, the three discernible Q values are confirmed for both Jade and fused-silica structural models generated from force-enhanced atomic-refinement (FEAR) simulations [11]. The positions of the FSDPs of the three grouped structure

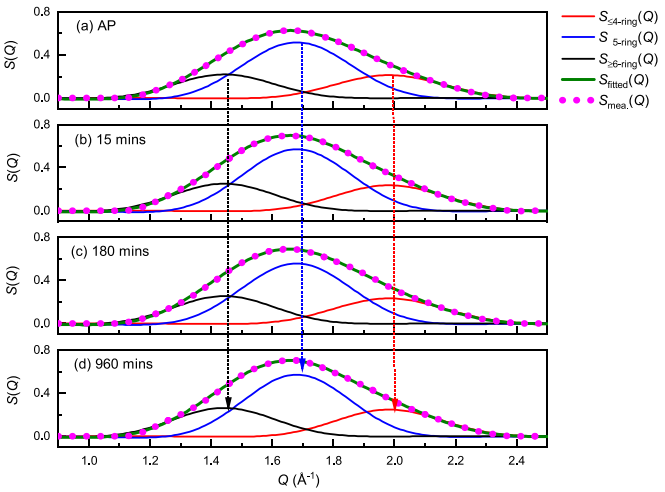

FIG. 3. First sharp diffraction peak (FSDP) deconvolution of thermally annealed glasses by the RingFSDP method [10]. $S_{\leqslant 4\text{-ring}}(Q)$ (red) is the Q-range component of $\leqslant 4$ rings with a corresponding real-space position of 3.15 Å; $S_{5\text{-ring}}(Q)$ (blue) and $S_{\geqslant 6\text{-ring}}(Q)$ (black) have real-space positions of 3.70 and 4.30 Å, respectively. The sum of all three $S_{\mathrm{n\text{-}ring}}(Q)$ functions (solid green curve) matches with the measured $S(Q)$-FSDP with the background removed (dotted pink curve). The three fixed positions with the values of 2.00, 1.70, and 1.46 Å^{-1}, are shown by the three straight vertical dotted lines, corresponding to the real-space characteristic periodicities of 3.15, 3.70, and 4.30 Å, respectively.

factors (i.e., $\leqslant 4-$, $5-$, and $\geqslant 6-$membered rings) calculated from FEAR-based structures exhibit very good agreement with the three fixed-Q values that were empirically derived from the FSDP deconvolution of 81 silicate glasses [10]. This confirmation not only provides a strong validation of the RingFSDP method but also implies that a reliable deconvolution of the FSDP can be achieved involving only six fitting parameters (i.e., the intensities and widths of the three Gaussian distributions) rather than nine (i.e., if three additional fitting parameters were to be needed for the positions).

In the reciprocal-space function $S(Q)$, the integrated area of each peak is proportional to the absolute number of such specified size rings, wherein the shape of the ring exhibits a certain minimum level of ordering (i.e., poorly ordered rings are assumed not to contribute to the peak). Such a level of ordering is discussed in Sec. III C. The relative ring-size distribution ($f_{n\text{-ring}}$) is calculated from the ratio of the integrated peak area [$A_{S_{n\text{-ring}}(Q)}$] to the total FSDP area [$A_{S_{\mathrm{FSDP}}(Q)}$] using Eq. (1):

$$f_n = \frac{A_{S_{n\text{-ring}}(Q)}}{A_{S_{\mathrm{FSDP}}(Q)}}. \tag{1}$$

Then the average (ave.) MRD in real space can be calculated as

$$\text{ave. MRD (Å)} = f_{\leqslant 4\text{-ring}} \times 3.15 + f_{5\text{-ring}} \times 3.70 + f_{\geqslant 6\text{-ring}} \times 4.30. \tag{2}$$

As shown in Fig. 3, the FSDP of the AP and three thermally annealed glasses can be deconvolved into three different ring-size groups by the RingFSDP method [10], and

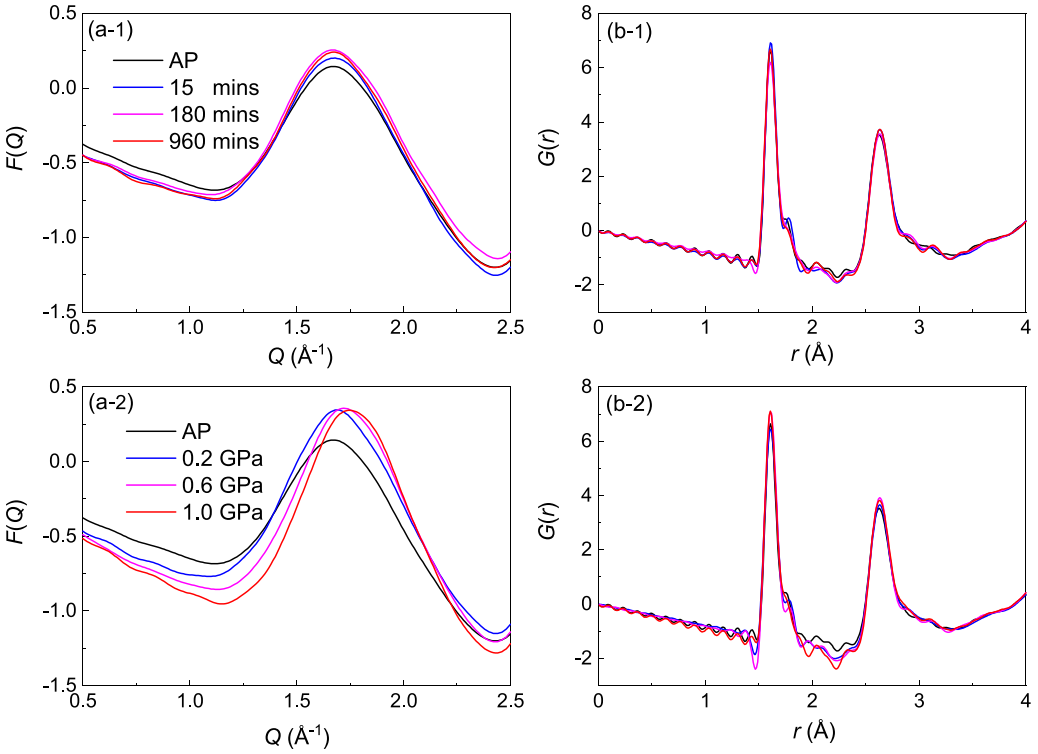

FIG. 4. (a-1) and (a-2) Zoomed $F(Q)$−first sharp diffraction peak (FSDP) and (b-1) and (b-2) zoomed $G(r)$ with nearest atomic pairs of A-O and O-O correlations from AO_4 tetrahedra for thermally annealed (top panel) and pressure-quenched (bottom panel) glasses. Differences are observed in the FSDPs for both treatment series, which are especially significant for pressure-quenched glasses. No observable differences are shown in the short-range AO_4 tetrahedral configuration in the $G(r)$ curves.

the related structural information is listed in Supplemental Material Table S1 [16]. Good fits are achieved for all four patterns, with a reduced mean-square-error of $\chi^2 < 1.9 \times 10^{-6}$. For each dataset, three individual peaks corresponding to the three ring-size groups are plotted; the sum (solid green curve) is in good agreement with the experimental FSDP (dotted pink curve). The peak positions of the three $F(Q)'$s of 2.00, 1.70, and 1.46 Å^{-1} are shown by the three straight vertical dotted lines, whose reciprocals ($2\pi/Q$) are consistent with the three real-space characteristic lengths ($r_{\leqslant 4\text{-ring}} = 3.15$ Å, $r_{5\text{-ring}} = 3.70$ Å, and $r_{\leqslant 6-\text{ring}} = 4.30$ Å), as described earlier.

The rings of the pressure-quenched glasses are compressed; thus, the three positions of the Gaussian peaks should increase accordingly for FSDP deconvolution. However, a direct refinement of a total of nine parameters (three positions, three heights, and three widths) does not lead to a reliable fitting because the nine parameters are heavily correlated with each other. Here, we still apply the RingFSDP method to refine six height and width parameters with three fixed positions. Even though this is not physically correct, our goal is to determine the ave. MRD at each specified pressure MRD_P (P represents the pressure) using Eq. (2). A series of FEAR simulations [11] of pressure-quenched glasses are in process to further explore how the sizes of small, intermediate, and large rings depend on the applied pressure. The peak positions of the three $F(Q)'$s will be determined from the simulated structure, then used to quantify the ring-size distribution from experimental neutron data by applying the RingFSDP method. That will enable us to study the change of different sized rings upon varying pressure and correlate this structural feature with the change in hardness.

The error in the RingFSDP analysis comprises many factors: sample preparation and alignment, beam-intensity fluctuation, instrumental calibration, counting statistics, data normalization, and FSDP fitting. It is challenging to evaluate the contribution of each individual factor and then mathematically propagate the error. Here, as an alternative path, we apply an easy but not statistically accurate method by using reproductivity value as an error estimation of the RingFSDP analysis. That is, two fused silica (FS) samples were prepared from the same piece of glass and measured during two beam-times. Each dataset was normalized and analyzed by the RingFSDP method. The differences between the two datasets, in terms of position and integrated area of $S(Q)$-FSDP, are listed in Supplemental Material Table S1 [16] and used as the error values of this study. This method would be more relevant using Jade glass; however, only data for FS data were collected here.

III. RESULTS

A. Rigid-unit modes

The FSDP regions of $F(Q)$ of all glasses are plotted in Figs. 4(a-1) and 4(a-2). Zoomed-in $G(r)$ functions with nearest atomic pairs of A-O and O-O from AO_4 tetrahedra (A = Si or Al) are plotted in Figs. 4(b-1) and 4(b-2) for thermally annealed (top panel) and pressure-quenched (bottom panel) glasses. No observable differences are evident in the A-O and O-O atomic-pair correlations for all seven glasses, in

terms of peak position corresponding to atomic-pair length and peak width corresponding to the deviation of atomic-pair length. This indicates that all glasses should have same O-*A*-O bond-angle distribution, which disproves the first MD simulated result that the standard deviations of the O-*A*-O bond-angle increase as a function of pressure for pressure-quenched glasses, as shown in fig. 4 of Ref. [14]. Since the high-density glasses cannot be made experimentally by the thermal-annealing process, we do not have the *A*-O and O-O atomic-pair correlation data for high-density thermally annealed glasses; we cannot comment on the second MD observation, the standard deviations of the O-*A*-O bond-angle decrease as a function of annealing time for thermal-annealed glasses. However, the pressure-independent, constant O-*A*-O bond-angle distributions lead us to question the third MD observation that, for glasses with similar densities, the standard deviation of the O-*A*-O bond angle is smaller for glass made by thermal annealing than by the pressure-quenching process. The *A*-O-*A* bond-angle distribution cannot be derived because the *A*-*A* atomic pair, in the range of 3.0–3.3 Å, is strongly overlayed by the high-*r* tail of the O-O pair.

The average oxygen coordination number around network-former atoms *A*, obtained from integration of the first *A*-O peak in the radial distribution function $R(r)$ $[R(r) = 4\pi r^2\rho_0 + rG(r)]$ [20], is 4.0 ± 0.1 for all glasses, indicating that the AO_4 tetrahedra remain intact after undergoing both thermal and pressure treatments. This is also supported by nuclear magnetic resonance (NMR) measurements. Although NMR tests were not performed for this series of Jade glasses, ^{27}Al MAS NMR analyses conducted on sodium aluminosilicate glasses show all the Al atoms maintain a tetrahedral configuration and are insensitive to annealing- or pressure-induced compaction [21]. Although an increase in coordination number has been reported for a wide variety of network formers (including B, Si, Ge, or Al) at high-pressure (>5 GPa) [22,23], the highest pressure used in this paper was only 1 GPa, which is not high enough to induce any increase in the coordination number of Si and Al atoms.

The observed intact tetrahedral short-range structure is in line with the rigid-unit mode (RUM) theory of network silicate crystals [24,25] or glasses [26,27]. The basic idea of the RUM approach is that the intra-AO_4 tetrahedral forces (*A*-O stretching and O-*A*-O bending) are much stronger than the intertetrahedral forces (the corner-linked *A*-O-*A*-O torsion or intertetrahedral *A*-O-*A* bending). A very high-energy penalty is required to distort a tetrahedron; therefore, it should be treated as a rigid unit. Instead, low-energy deformations are achieved by intertetrahedral *A*-O-*A* deformations, including both bond-angle and dihedral torsion-angle changes [28]. The rotations are believed to lead to changes in ring shape, such as distortion or buckling or, in contrast, in transitions from a distorted or buckled shape to a more ordered symmetric and flatter one. This is in turn reflected as a medium-range structural change—the FSDP change. As shown in Figs. 4(a-1) and 4(a-2), differences are observed in the FSDPs for both treatment series of glasses. They are especially significant for pressure-quenched glasses, with peak-position shifts, peak-area increases, as well as FSDP shape changes, shown as the nontranslation peak skewing, which shifts more in the low-Q region and less in the high-Q region. Since in this paper the peak positions of different sized ring groups have not been determined for pressure-quenched glasses, only the FSDP position and area, not the shape, are analyzed. The medium-range structure information, derived by the RingFSDP analysis, is summarized in Supplemental Material Table S1 [16].

B. FSDP-position change

The real-space ave. MRDs of all glasses are calculated, based on their reciprocal-space FSDP deconvolution results, using Eq. (2), respectively, and listed in Supplemental Material Table S1 [16]. The relative changes in ave. MRD (with respect to the value of the AP glass) are plotted in Fig. 5(a) as a function of their corresponding thermal-annealing duration (red, lower x axis) or compression pressure (blue, upper x axis). The ave. MRD does not noticeably change upon thermal annealing but decreases linearly with pressure. For an easy comparison, the changes in density (ρ) are plotted in Fig. 5(b). An inverse linear property-structure correlation between ρ and the ave. MRD change, with a slope close to -1, is observed in Fig. 5(c). As the MRD decreases, the glass becomes more packed, with a higher density. However, the value of the ave. MRD change represents a one-dimensional linear compression, while the change in ρ reflects a three-dimensional volumetric change. For an isotropic crystalline material, the volumetric coefficient of thermal expansion (CTE) is three times of the linear CTE, while an area CTE would be two times the linear CTE. If the MRD compression was the only factor governing the change in bulk ρ, the slope should be -2 (if the compression is two-dimensional and occurs within the approximate plane of each ring) or -3 (if the compression occurs along the three dimensions) but not -1. The fact that the bulk ρ increases by less than what is expected (from the decrease in the MRD) implies the existence of other structural changes that play an opposite role for volume compression, such as changes in the ring shape. The nearly 1:1 relation between volumetric and linear compression is in line with our previous study, in which some discrepancies were observed among microscale short-range, medium-range, and macroscale bulk values of the CTE for FS glass [29].

C. FSDP-area change

The relative changes in the integrated $S(Q)$-FSDP area (with respect to the value obtained for the AP glass) are plotted in Fig. 6(a) as a function of their corresponding thermal-annealing duration (red, lower x axis) or compression pressure (blue, upper x axis). The $S(Q)$-FSDP area increases both upon thermal annealing and pressure quenching. For comparison, the changes in hardness (H) are plotted in Fig. 6(b). Despite the large error bars associated with the variations in H, a positive property-structure correlation can still be observed between H and the $S(Q)$ area, as shown in Fig. 6(c). Two sets of hardness values are plotted in Fig. 6(c) for the pressure-quenched glasses: the blue ones are from the original hardness values, whereas the black ones are modified hardness values, corrected to filter out densification effects

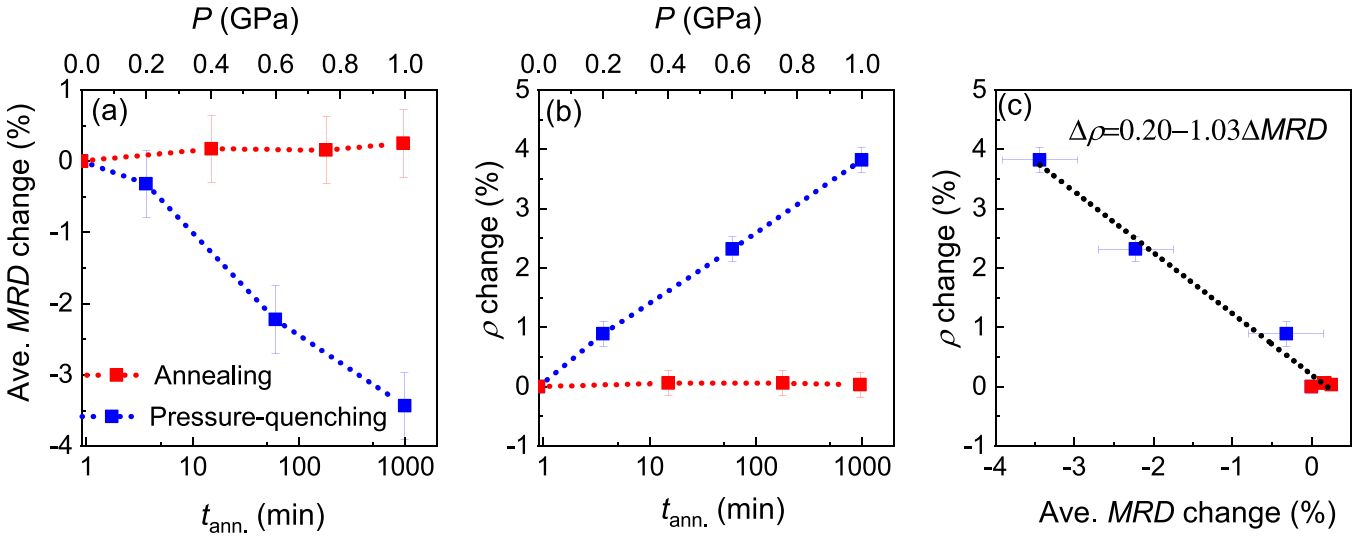

FIG. 5. Thermal-annealing (red) and pressure-quenching (blue) effects on the change in (a) average medium-range distance (ave. MRD) and (b) density (ρ). (c) highlights a linear property-structure correlation between ρ and ave. MRD. The relative change (%) is calculated by comparing each treated glass with the same as-prepared glass. The ave. MRD does not change upon annealing but decreases linearly with pressure. The dotted lines in (a) and (b) are guides for the eye; that in (c) is a least-squares fit. The errors in the ave. MRD change are propagated from the difference of ave. MRD values obtained by two neutron total-scattering measurements performed on two separate samples of the same fused silica glass.

using Eq. (3):

$$\Delta H/H(\%) = \frac{H_P/\rho_P - H_{AP}/\rho_{AP}}{H_{AP}/\rho_{AP}} \times 100. \quad (3)$$

To interpret the correlation between the $S(Q)$-FSDP area increase and the increase in H, we first discuss what kinds of changes in ring structure can lead to the FSDP area increase. The most obvious candidate would be an increase in the number of rings, i.e., more rings are formed by thermal or pressure treatments. However, the ring-number increase interpretation goes against both RUM theory and simulation results [30,31]. Indeed, our neutron-scattering results already demonstrate that the network silicate glasses satisfy the RUM theory on account of the intact short-range AO_4 tetrahedra and very flexible medium-range ring structure in response to increased temperature [29,32] and pressure changes in this study. Therefore, the structural change resulting from thermal annealing or pressure should follow the deformation path

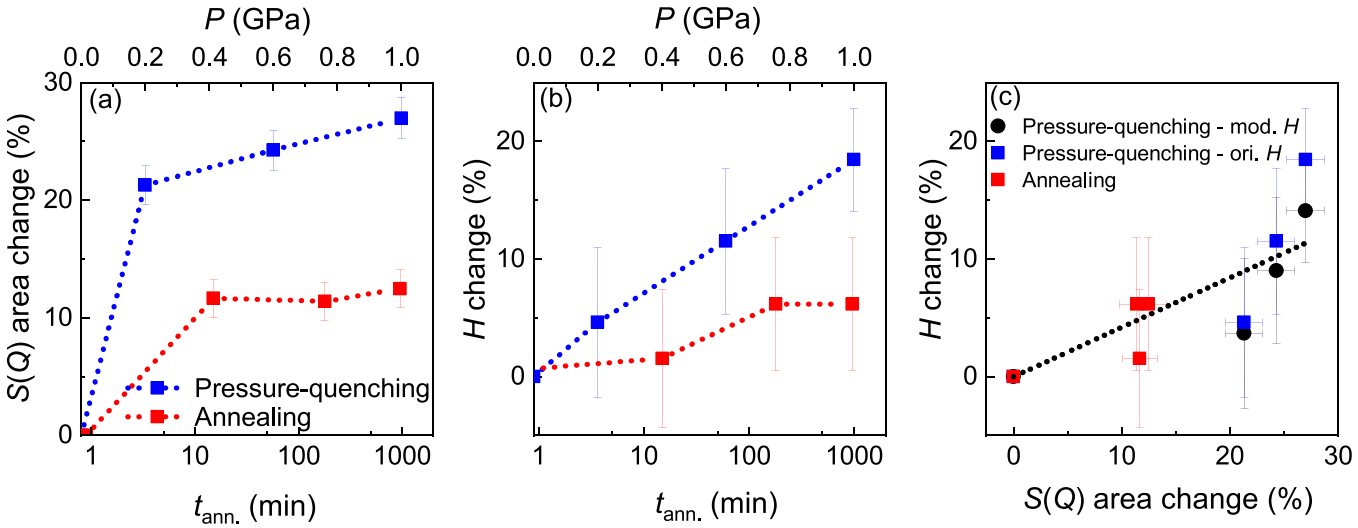

FIG. 6. Thermal-annealing (red) and pressure-quenching (blue) effects on the change of (a) integrated $S(Q)$-first sharp diffraction peak (FSDP) area and (b) hardness (H). (c) highlights a positive property-structure correlation between H and the $S(Q)$-FSDP area. The relative change (%) is calculated by comparing each treated glass with the as-prepared one. Two sets of hardness values are plotted in (c) for pressure-quenched glasses: the blue ones are from original hardness values, whereas the black ones are the modified hardness values, corrected to filter out densification effects. The errors in the $S(Q)$-FSDP area change values are propagated from the difference of $S(Q)$ area values obtained by two neutron total-scattering measurements of two separate samples of the same fused silica glass.

associated with the lowest cost in energy, such as the intertetrahedral *A*-O-*A* angular deformations. In contrast, a change in the number of rings would require some *A*-O bonds to break and reform, which involves much higher energy barriers and is, therefore, unlikely to happen when a low-energy barrier (*A*-O-*A* rotation) pathway exists for the system to deform. Moreover, simulation results on sodium silicate glasses $[(Na_2O)_{30}(SiO_2)_{70}]$ prepared with four orders of magnitude different cooling rates [30] and MD-RMC modeling on cold- and hot-pressed fused-silica glasses [31] also demonstrate that even glasses exhibiting significant differences in their FSDP tend to show negligible differences in their numbers of rings.

We then turn to another possibility—a change in ring shape. To this end, we explore how the rings contribute to constructive diffraction that eventually leads to the FSDP. A real-space–reciprocal-space analysis, combining a continuous wavelet-transform analysis and MD simulations, has demonstrated that the medium-range-order-related FSDP in FS is manifested by interatomic distances in the region of $r \sim 5$ Å, associated with a couple of local pseudo-Bragg planes [33]. Such near-parallel local planes are formed by both Si and O atoms from the second-nearest neighbors. The perpendicular distance between the parallel planes can result in constructive diffraction, leading to the FSDP in $S(Q)$. Small-sized rings exhibit shorter distances between planes, whereas larger-sized rings correspond to longer distances, as confirmed in Ref. [11]. Only near-parallel planes will contribute to the FSDP. If a ring has a shape that is too skewed or distorted from the averaged ring shape, it can be assumed that it will not contribute significantly to the FSDP, even if the ring itself is still intact. Both the thermal and pressure processes applied in this study provide annealing treatments that can make the glass structure more relaxed, thereby possibly making the ring shape less buckled or distorted and allowing more contribution to the FSDP with a correspondingly increased FSDP area. This is in line with our experimental observation that the FSDP area decreases with increasing temperature [29,32] since heating reduces the structural ordering, an opposite effect from sub-T_g annealing, which increases the ordering.

The energy barrier to activate a permanent deformation, following the definition of hardness, would be higher if a glass has a more ordered structure since extra energy would be needed to deform the ordered structure into a distorted state before reaching the permanent deformation. Therefore, we speculate that a glass with a more ordered structure resulting from annealing or pressure—as reflected in the increase in the area of the FSDP—needs to overcome higher energy barriers to reach a permanent deformation, which in turn leads to a higher hardness.

IV. DISCUSSIONS

Overall, in this paper, we reveal the existence of an intimate relationship between medium-range structural order and hardness in glasses, i.e., the increased level of order in the medium range is the structural origin of the extra extent of hardness increase; that is, it explains why hardness increases more than what would be expected when solely accounting for the effect of densification. However, assessing the level of order in the medium range, as captured in this paper by the integrated area of the FSDP, cannot be used to compare glasses with different compositions due to its composition-dependent nature. Indeed, the FSDP area is proportional to the weighted sum (using the neutron scattering lengths as weights) of all the contributions of each interatomic pair. Although both experiments [10] and simulations [11] have demonstrated that the FSDP originates from the network-forming rings in the atomic structure, the exact contribution by each type of atomic pair (such as *A*-O, O-O, *A*-*A*, or any of their combinations) remains unknown.

In contrast, the ring size distribution itself can be used to decode the nature of the correlation between glass hardness and chemical composition since, in this case, the neutron scattering length is cancelled out in the calculation, as shown by Eq. (1). This approach has been used to successfully interpret the abnormal deviation from linearity in the hardness of certain silicate glasses [8,9]. That is, for fully compensated calcium aluminosilicate glasses with equal molar contents of CaO and Al_2O_3, the hardness decreases upon increasing silica content until 70 mol. % and then increases with silica content. In general, the hardness of normal silicate glasses increases upon increasing packing fraction. In contrast, it is well established that silica-rich glasses exhibit an anomalous behavior in their mechanical and thermal properties [9,34,35], as they present an inverse correlation between hardness and packing fraction. For low-SiO_2 glasses (with SiO_2 content < 70 mol. %, normal glasses), hardness increases with increased packing fraction and decreasing SiO_2 content. In contrast, the opposite behavior is observed for high-SiO_2 glasses (anomalous glasses), wherein hardness increases upon decreasing packing fraction and increasing SiO_2 content. The transition between these two regimes occurs near 70 mol. % SiO_2 [8]. This anomalous behavior is generally explained by a transition in deformation mechanisms, namely, silica-poor glasses exhibit significant volume-displacing shear deformation shown as median/radial and lateral cracks [35], whereas silica-rich glasses tend to exhibit volume-reducing densification shown as ring/cone cracks [35]. In that regard, our previous RingFSDP study [10] demonstrated that, at the $\sim$ 70 mol. % SiO_2 transition point, large-sized rings begin to emerge, and their relative fraction continues to increase as the SiO_2 content increases. We speculate that the higher content of large-sized rings leads to a more open structure which, in turn, is associated with a higher capability for the glass to be elastically compressed while resisting plastic flow, thereby resulting in a higher hardness.

We compare the correlation of medium-range structure with physical properties (density and hardness) between normal and abnormal glass-FS. FS is identified as abnormal because its density (ρ) increases as the fictive temperature T_f increases, while for normal glass, ρ decreases as T_f increases. Based on the x-ray total scattering analysis of FS at different T_f [36], as well as our neutron measurements of alkaline-earth aluminosilicate glass annealed at different temperature for different durations (Supplemental Material [16]), we list the signs of parameter-T_f dependence ($d\text{Parameter}/dT_f$) in Table I, where a positive sign indicates that the value of that parameter increases as T_f increases, and a negative sign indicates that the value of that parameter decreases as T_f increases. Both abnormal and normal glasses show the same

TABLE I. Signs of T_f dependence of medium-range structure and properties parameters. Positive sign + means the parameter value increases as T_f increases; negative sign − means the parameter value decreases as T_f increases.

	Medium-range structure				
	Length-related packing fraction			Properties	
Glass type	Ordering (FSDP area)	Reciprocal space (FSDP position)	Real space (MRD)	Density (ρ)	Hardness (H)
Normal	−	−	+	−	−
Abnormal	−	+	−	+	+

medium-range structure ordering change, i.e., become less ordering (negative sign) as T_f increases, which is normal, as expected. In contrast, they show opposite MRD change: MRD of normal glass increases as T_f increases, as illustrated in the Supplemental Material [16], while MRD of abnormal glass decreases as T_f increases [36]. Except the MRD parameter, both normal and abnormal glasses follow the same two universal rules which govern the structure-property correlation: (1) inverse correlation between MRD density ρ; larger MRD leads to lower ρ; and (2) positive correlation between density ρ and hardness H, interpreted as higher ρ, higher packing fraction and elastic modulus, then higher H [37]. Therefore, the only abnormal part of FS glass is the positive MRD-T_f correlation, which has been studied extensively but remains elusive [38,39]. Except this, everything else remains normal for the abnormal FS.

V. CONCLUSIONS

In this paper, we have confirmed the applicability of RUM theory [26] for silicate glasses, based on the short- and medium-range structural information derived from the structure factor obtained from neutron total scattering. Short-range SiO_4 and AlO_4 tetrahedra are observed to remain intact among all the aluminosilicate glasses studied, independently of the thermal or pressure treatment, whereas medium-range ring structures are found to exhibit some variation, as reflected in significant observed changes in the FSDP in the neutron-scattering structure factor. Close correlations are observed between physical properties and the medium-range structure, as captured by some changes in the position and intensity of the FSDP of the neutron structure factor. Specifically, (1) the density variation is inversely proportional to the ave. MRD change, derived from the shift in FSDP position; and (2) a positive correlation is observed between the hardness increase and the medium-range order increase, revealed by the integrated FSDP area increase.

The medium-range structure, specially represented as ring size distribution, could be applied as a basis to decipher changes in other properties involving atomic-level plastic structural deformation, such as fragility, as well as to understand the origin of the variation in the glass-transition temperature for field strength modifiers [40].

The Python program RingFSDP was used to derive ring-structure information from neutron-scattering FSDPs. It can batch process $F(Q)$ files to acquire $I(r)$ of FSDPs, profile fit $I(r)$, inverse Fourier transform to get $F_n(Q)$, derive $S_n(Q)$, and integrate and calculate total and n-membered ring numbers. The code is available from the NOMAD beamline upon request.

ACKNOWLEDGMENTS

Y.S. used resources at the SNS, a U.S. Department of Energy Office of Science User Facility operated by the Oak Ridge National Laboratory. M.B. acknowledges funding from the National Science Foundation under Grants No. CMMI-1826420 and No. DMR-1928538.

[1] M. Ren, J. Cheng, S. P. Jaccani, S. Kapoor, R. E. Youngman, L. Huang, J. Du, and A. Goeal, Composition-structure-property relationships in alkali aluminosilicate glasses: a combined experimental-computational approach towards designing functional glasses, J. Non-Cryst. Solids **505**, 144 (2019).

[2] Y. Shi, A. Tandia, B. Deng, S. R. Elliott, and M. Bauchy, Revisiting the Makishima-Mackenzie model for predicting the Young's modulus of oxide glasses, Acta Mater. **195**, 252 (2020).

[3] Y. H. Yun and P. J. Bray, Nuclear magnetic resonance studies of the glasses in the system Na_2O-B_2O_3-SiO_2, J. Non Cryst. Solids **27**, 363 (1978).

[4] L. Deng and J. Du, Development of boron oxide potentials for computer simulations of multicomponent oxide glasses, J. Am. Ceram. Soc. **102**, 2482 (2019).

[5] J. O. Byun, B. H. Kim, K. S. Hong, H. J. Jung, S. W. Lee, and A. A. Izyneev, Properties and structure of RO-Na_2O-Al_2O_3-P_2O_5 (R = Mg, Ca, Sr, Ba) glasses, J. Non-Cryst. Solids **190**, 288 (1995).

[6] C. J. Wilkinson, A. R. Potter, R. S. Welch, C. Bragatto, Q. Zheng, M. Bauchy, M. Affatigato, S. A. Feller, and J. C. Mauro, Topological origins of the mixed alkali effect in glass, J. Phys. Chem. B **123**, 7482 (2019).

[7] J. Kjeldsen, M. M. Smedskjaer, J. C. Mauro, R. E. Youngman, L. Huang, and Y. Yue, Mixed alkaline earth effect in sodium aluminosilicate glasses, J. Non-Cryst. Solids **369**, 61 (2013).

[8] L. Lamberson, Influence of atomic structure on plastic deformation in tectosilicate calcium-aluminosilicate, magnesium-aluminosilicate, and calcium-galliosilicate glasses, Ph.D. thesis, Cornell University, 2016.

[9] M. Kazembeyki, K. Yang, J. C. Mauro, M. M. Smedskjaer, M. Bauchy, and C. G. Hoover, Decoupling of indentation modulus and hardness in silicate glasses: evidence of a shear- to densification-dominated transition, J. Non-Cryst. Solids **553**, 120518 (2021).

[10] Y. Shi, J. Neuefeind, D. Ma, K. Page, L. A. Lamberson, N. J. Simith, A. Tandia, and A. P. Song, Ring size distribution

in silicate glasses revealed by neutron scattering first sharp diffraction peak analysis, J. Non-Cryst. Solids **516**, 71 (2019).

[11] Q. Zhou, Y. Shi, B. Deng, J. Neuefeind, and M. Bauchy, Experimental method to quantify the ring size distribution in silicate glasses and simulation validation thereof, Sci. Adv. **7**, 28 (2021).

[12] W. C. Oliver and G. M. Pharr, An improved technique for determining hardness and elastic modulus using load and displacement sensing indentation experiments, J. Mater. Res. **7**, 1564 (1992).

[13] T. To, L. R. Jensne, and M. M. Smedskjaer, On the relation between fracture toughness and crack resistance in oxide glasses, J. Non-Cryst. Solids **534**, 119946 (2020).

[14] M. M. Smedskjaer, M. Bauchy, J. C. Mauro, S. J. Rzoska, and M. Bockowski, Unique effects of thermal and pressure histories on glass hardness: structural and topological origin, J. Chem. Phys. **143**, 164505 (2015).

[15] M. Potuzak, J. C. Mauro, T. J. Kiczenski, A. J. Ellison, and D. C. Allan, Resolving the vibrational and configurational contributions to thermal expansion in isobaric glass-forming systems, J. Chem. Phys. **133**, 091102 (2010).

[16] See Supplemental Material at http://link.aps.org/supplemental/10.1103/PhysRevMaterials.7.013602 for revealing the effect of medium-range structure on silicate glass hardness.

[17] M. M. Smedskjaer, S. J. Rzoska, M. Bockowski, and J. C. Mauro, Mixed alkaline earth effect in the compressibility of aluminosilicate glasses, J. Chem. Phys. **140**, 054511 (2014).

[18] J. Neuefeind, M. Feygenson, J. Carruth, R. Hoffmann, and K. Chipley, The nanoscale ordered materials diffractometer NOMAD at the spallation neutron source SNS, Nucl. Instrum. Methods Phys. Res. B **287**, 68 (2012).

[19] Y. Shi, N. T. Lonnroth, Youngman R. E., S. J. Rzoska, M. Bockowski, and M. M. Smedskjaer, Pressure-induced structural changes in titanophosphate glasses studied by neutron and x-ray total scattering analyses, J. Non-Cryst. Solids **483**, 50 (2018).

[20] D. A. Keen, a comparison of various commonly used correlation functions for describing total scattering, J. Appl. Cryst. **34**, 172 (2001).

[21] M. N. Svenson, L. M. Thirion, R. E. Youngman, J. C. Mauro, M. Bauchy, S. J. Rzoska, M. Bockowski, and M. M. Smedskjaer, Effects of thermal and pressure histories on the chemical strengthening of sodium aluminosilicate glass, Front. Mater. **3**, 14 (2016).

[22] P. S. Salmon and A. Zeidler, Networks under pressure: the development of *in situ* high-pressure neutron diffraction for glassy and liquid materials, J. Phys.: Condens. Matter. **27**, 133201 (2015).

[23] A. Zeidler and P. S. Salmon, Pressure-driven transformation of the ordering in amorphous network-forming materials, Phys. Rev. B **93**, 214204 (2016).

[24] A. P. Giddy, M. T. Dove, G. S. Pawley, and V. Heine, The determination of rigid unit modes as potential soft modes for displacive phase transitions in framework crystal structures, Acta Cryst. **A49**, 697 (1993).

[25] K. D. Hammonds, M. T. Dove, A. P. Giddy, V. Heine, and B. Winkler, Rigid unit phonon modes and structural phase transitions in framework silicates, Am. Mineral. **81**, 1057 (1996).

[26] M. T. Dove, K. D. Hammonds, M. J. Harris, V. Heine, D. A. Keen, A. K. A. Pryde, K. O. Trachenko, and M. C. Warren, Amorphous silica from the rigid unit mode approach, Mineral. Mag. **64**, 377 (2000).

[27] U. Buchenau, N. Nucker, and A. J. Dianoux, Neutron Scattering Study of the Low-Frequency Vibrations in Vitreous Silica, Phys. Rev. Lett. **53**, 2316 (1984).

[28] M. Wang, B. Wang, T. K. Bechgaard, J. C. Mauro, S. J. Rzoska, M. Bockowski, M. M. Smedskjaer, and M. Bauchy, Crucial effect of angular flexibility on the fracture toughness and nanoductility of aluminosilicate glasses, J. Non-Cryst. Solids **454**, 46 (2016).

[29] Y. Shi, D. Ma, A. P. Song, B. Wheaton, M. Bauchy, and S. R. Elliott, Structural evolution of fused silica below the glass-transition temperature revealed by *in-situ* neutron total scattering, J. Non-Cryst. Solids **528**, 119760 (2020).

[30] X. Li, W. Song, K. Yang, N. M. Anoop Krishnan, B. Wang, M. M. Smedskjaer, J. C. Mauro, G. Sant, M. Balonis, and M. Bauchy, Cooling rate effects in sodium silicate glasses: bridging the gap between molecular dynamics simulations and experiments, J. Chem. Phys. **147**, 074501 (2017).

[31] Y. Onodera, S. Kohara, P. S. Salmon, A. Hirata, N. Nishyama, S. Kitani, A. Zeidler, M. Shiga, A. Masuno, H. Inoue *et al.*, Structure and properties of densified silica glass: characterizing the order within disorder, NPG Asia Mater. **12**, 85 (2020).

[32] Y. Shi, O. Gulbiten, J. Neuefeind, M. Dong, A. P. Song, B. Wheaton, M. Bauchy, and S. R. Elliott, Temperature-induced structural change through the glass transition of silicate glass by neutron diffraction, Phys. Rev. B **101**, 134106 (2020).

[33] T. Uchino, J. D. Harrop, S. N. Taraskin, and S. R. Elliott, Real and reciprocal space structural correlations contributing to the first sharp diffraction peak in silica glass, Phys. Rev. B. **71**, 014202 (2005).

[34] A. Arora, D. B. Marshall, and B. R. Lawn, Indentation, deformation/fracture of normal and anomalous glasses, J. Non-Cryst. Solids **31**, 415 (1979).

[35] T. M. Gross, Deformation and cracking behavior of glasses indented with diamond tips of various sharpness, J. Non-Cryst. Solids **358**, 3445 (2012).

[36] H. Masai, S. Kohara, Y. Onodera, A. Koreeda, K. Saito, E. H. Sekiya, and N. Kitamura, Relationship between the first sharp diffraction peak and physical properties of silicon dioxide (SiO_2) glasses possessing different fictive temperatures, J. Ceram. Soc. Jpn. **128**, 1038 (2020).

[37] T. M. Gross and M. TomoZawa, Fictive temperature-independent density and minimum indentation size effect in calcium aluminosilicate glass, J. Appl. Phys. **104**, 063529 (2008).

[38] R. Bruckner, Properties and structure of vitreous silica. I, J. Non-Cryst. Solids **5**, 123 (1970).

[39] L. Huang and J. Kieffer, Amorphous-amorphous transitions in silica glass. I. Reversible transitions and thermomechanical anomalies, Phys. Rev. B **69**, 224203 (2004).

[40] A. Atila, E. M. Ghardi, S. Ouaskit, and A. Hasnaoui, Atomistic insights into the impact of charge balancing cations on the structure and properties of aluminosilicate glasses, Phys. Rev. B **100**, 144109 (2019).